Algorithm 975: TMATROM—A T-Matrix Reduced Order Model Software

M. GANESH, Colorado School of Mines
S. C. HAWKINS, Macquarie University

The T-matrix (TMAT) of a scatterer fully describes the way the scatterer interacts with incident fields and scatters waves, and is therefore used extensively in several science and engineering applications. The T-matrix is independent of several input parameters in a wave propagation model and hence the offline computation of the T-matrix provides an efficient reduced order model (ROM) framework for performing online scattering simulations for various choices of the input parameters. The authors developed and mathematically analyzed a numerically stable formulation for computing the T-matrix (J. Comput. Appl. Math. 234 (2010), 1702–1709). The TMATROM software package provides an object-oriented implementation of the numerically stable formulation and can be used in conjunction with the user's preferred forward solver for the two-dimensional Helmholtz model. We compare TMATROM with standard methods to compute the T-matrix for a range of two-dimensional test scatterers with large aspect ratios and acoustic sizes. Our numerical results demonstrate the robust numerical stability of the TMATROM implementation, even with scatterers for which the standard methods are numerically unstable. The efficiency and flexibility of the TMATROM software package to handle a wide range of two-dimensional scatterers with various shapes and material properties are also demonstrated.

CCS Concepts: ● **Mathematics of computing** → **Solvers**; **Partial differential equations**

Additional Key Words and Phrases: T-matrix, acoustic scattering, far field, numerical stability

1. INTRODUCTION

We evaluate the numerical performance of our object-oriented Matlab package TMA-TROM for computing the transition matrix (T-matrix) for efficient simulation of wave scattering in two dimensions. The package is described in detail in the accompanying user manual [Ganesh and Hawkins 2016]. The T-matrix of a wave propagation model is independent of various typical input parameters (such as those determining the incident wave) and hence provides an efficient framework for performing online scattering simulations for various choices of the input parameters. This approach is particularly useful for parameter-dependent multiple scattering configurations, especially dynamic configurations or uncertain configurations.

9

The TMATROM package implements the authors' numerically stable algorithm [Ganesh and Hawkins 2009] for computing the T-matrix of a two-dimensional scatterer. Routines required to use the T-matrix for a range of scattering problems—such as scattering by configurations with several scatterers (see Ganesh and Hawkins [2016, Section 8])—are also implemented, including evaluation of regular and radiating wavefunction expansions, and the translation-addition theorem (see Ganesh and Hawkins [2016, Sections 5–7]).

The two-dimensional wave scattering model arises for various physical phenomena, including acoustic [Robertson and Rudy III 1998], electromagnetic [McPhedran et al. 1999; Little et al. 2015], or water waves [Tao et al. 2007; Montiel et al. 2015; Kagemoto and Yue 1986] interacting in three dimensions with cylinders (not necessarily with circular cross section). The two-dimensional model is also an important model for testing forward and inverse codes [Colton and Kress 2012, page 72]. The T-matrix method is particularly useful for parameter-dependent applications where simulations are required for multiple parameter values. Examples include monostatic cross section computations, multiple scattering, and stochastic problems [Ganesh and Hawkins 2013]. Consequently, this package will have extensive applications in several disciplines, including oceanography, physics, meteorology, and atmospheric science. We refer to the T-matrix reference database [Mishchenko et al. 2014] and the extensive references therein for particular applications of the T-matrix.

The T-matrix was first introduced in Waterman [1965]. Initially, the T-matrix was developed by Waterman for electromagnetic scattering by three-dimensional scatterers. In 1969, an acoustic scattering counterpart (in both two and three dimensions) was developed [Waterman 1969]. In Waterman's original works, the T-matrix was computed using the Null Field Method (NFM), which expands the surface field solution of the null field integral equation using regular (Rg) and radiating wavefunctions, and leads to the T-matrix in the form $-(\text{Rg}\,Q)\,Q^{-1}$ where $\text{Rg}\,Q$ and Q are square matrices whose entries are given by surface integrals involving regular and radiating wavefunctions, respectively. Offline computation and storage of the T-matrix facilitates fast online evaluation of the coefficients of the radiating scattered field using simple matrix-vector multiplication. Here the input data is the coefficient vector of the incident field.

Although the NFM is used extensively, it is well known that it is numerically unstable for scatterers that deviate significantly from a circle (e.g., scatterers that have a large aspect ratio) or are acoustically large [Somerville et al. 2012; Khlebtsov 2010]. The numerical instability is attributed to the integration of Hankel functions on the scatterer surface and manifests through poor conditioning of the matrix Q [Mishchenko and Travis 1994; Mishchenko et al. 1996; Petrov and Shkuratov 2007] and loss of precision in evaluating the entries in Q using quadrature [Waterman 2007, 2009; Somerville et al. 2012; Havemann and Baran 2004].

There is extensive literature concerned with strategies to avoid or mitigate the numerical instability in the NFM. The most general way to address loss of precision in the quadrature is to use extended precision arithmetic [Havemann and Baran 2004; Khlebtsov 2010]. However, for certain geometries—such as ellipses and capped cylinders—it is possible to enhance numerical stability by removing large leading order terms in the integrand that integrate to zero [Waterman 2007, 2009; Sarkissian et al. 1993; Somerville et al. 2013]. For ellipsoids, it is also possible to exploit symmetry in Q to obtain a more numerically stable expression [Waterman 1999].

Ill conditioning in Q has been addressed by subdividing Q to obtain better numerical stability in the matrix factorisation [Petrov and Shkuratov 2007] and by using extended precision arithmetic [Mishchenko and Travis 1994; Mishchenko et al. 1996]. Extended precision arithmetic is slow compared with the standard double precision arithmetic, and hence it is not desirable for large-scale applications. We are not aware of any double

precision implementation of the NFM that is numerically stable, without restrictions on the scatterer shape and acoustic size.

It is important to emphasize that the numerical difficulties discussed above relate to the computation of the T-matrix using the NFM, and numerical instability is not intrinsic to the T-matrix itself. Alternative methods to compute the T-matrix have been explored, including the invariant imbedding method [Bi et al. 2013], expansion of the surface field using discrete sources [Hellmers et al. 2011; Wriedt 2007], and methods based on point matching regular wavefunction expansions of the incident field with radiating wavefunction expansions of the scattered field on the scatterer boundary [Farafonov et al. 2010; Rother and Wauer 2010; Nieminen et al. 2003]. However, because the standard Point Matching Method (PMM) and its generalized form (GPMM) involve Hankel functions on the scatterer surface, they are also prone to numerical instability.

Freely available implementations of many of the above T-matrix algorithms for electromagnetic scattering in three dimensions are available, and many are listed on the Scattport website [Scattport 2016]. These include Fortran code implementing the NFM [Mishchenko 2000; Mishchenko and Travis 2007; Mishchenko 2016] and the NFM with discrete sources expansion of the surface field [Wriedt 2010]; and Matlab code implementing the NFM for ellipsoids [Somerville et al. 2016] and the GPMM [Nieminen et al. 2007; Nieminen 2014]. We are not aware of any freely available T-matrix software for scattering in two dimensions.

It has been recognized for a long time that numerical instability in T-matrix computations could be avoided by using a boundary integral method to compute the T-matrix [Martin 2003, Section 7.9.4]. The authors first developed a numerically stable formulation for the T-matrix using a boundary integral method for three-dimensional electromagnetic scattering [Ganesh and Hawkins 2010]. The authors also developed acoustic scattering counterparts for three dimensions [Ganesh and Hawkins 2008a] and two dimensions [Ganesh and Hawkins 2009].

The key to the numerical stability of the authors' formulation [Ganesh and Hawkins 2010, 2008a, 2009] is moving the computation of the T-matrix entries from the scatterer surface to the far field. In the far field, the Hankel functions are bounded and they present no numerical difficulties. The move from the near field (on the scatterer surface) to the far field requires simulation of the scattered fields induced by the interaction of regular wavefunctions with the scatterer surface. These simulations can be performed with any appropriate scattering algorithm.

The TMATROM package implements the authors' numerically stable algorithm [Ganesh and Hawkins 2009] using the Object Oriented (OO) features of Matlab. The OO design of the package (see Ganesh and Hawkins [2016, Section 2]) permits a choice of scattering algorithm using class inheritance from a solver base class. Classes implementing a high-order Nyström solver [Colton and Kress 2012, Section 3.5] and an open source solver (MPSPACK [Barnett and Betcke 2014]) are provided. Users may define their own classes to incorporate their own solvers (see Ganesh and Hawkins [2016, Part III]). This structure allows great flexibility in the shape and structure of the scatterers that can be modelled. In particular, there are no limitations on the shape of the scatterer provided a suitable algorithm is available for simulation of the scattered fields.

In this article, we demonstrate the TMATROM package by computing the T-matrix of several sound soft and sound hard test scatterers found in the literature. We show the enhanced numerical stability of TMATROM compared with the NFM and point matching methods. We also demonstrate the computational efficiency of the TMATROM code. For instructions on how to obtain, install, and use TMATROM, and also details on the structure and design of the software, we refer to the TMATROM manual [Ganesh and Hawkins 2016].

The article is structured as follows. In Section 2, we describe the two-dimensional scattering problem and define the T-matrix and associated wavefunction expansions. In Section 3, we briefly describe the NFM and the point matching methods. In Section 4, we briefly describe the numerically stable formulation for the T-matrix that we implement in TMATROM. In Section 5, we present detailed numerical results.

2. THE T-MATRIX METHOD

We consider the interaction of monochromatic time harmonic waves with a two-dimensional scatterer D. After suppressing $e^{-i\omega t}$ time dependence, where ω denotes the angular frequency, the associated spatially dependent field ψ satisfies the two-dimensional Helmholtz equation

$$\nabla^2 \psi + k^2 \psi = 0 \tag{1}$$

in the exterior of D where $k = 2\pi/\lambda$ is the wavenumber and λ is the wavelength. It is convenient to use polar coordinates (r, θ) with origin contained inside the scatterer D.

In the scattering problem, an incident field ψ^{inc} interacts with the scatterer to induce a scattered field ψ^{s}. Both fields satisfy the Helmholtz equation (1). The scattered field ψ^{s} additionally satisfies the Sommerfeld radiation condition [Colton and Kress 2012, Section 2.1]

$$\lim_{r \to \infty} r \left(\frac{\partial \psi^{\mathrm{s}}}{\partial r} - ik\psi^{\mathrm{s}} \right) = 0. \tag{2}$$

The corresponding far field ψ^{∞} of ψ^{s} is defined by

$$\psi^{\infty}(\theta) = \lim_{r \to \infty} \sqrt{r} e^{-ikr} \psi^{\mathrm{s}}(r, \theta). \tag{3}$$

In this work, we consider scattered fields induced by a boundary condition of the form

$$\mathcal{D}\psi = 0, \quad \text{on } \partial D, \tag{4}$$

where ∂D denotes the boundary of the scatterer D and $\psi = \psi^{\mathrm{s}} + \psi^{\mathrm{inc}}$ is the total field. The operator $\mathcal{D}$ depends on the material properties of the scatterer. For a sound soft scatterer $\mathcal{D}$ is the identity and for a sound hard scatterer $\mathcal{D}$ is the normal derivative on ∂D. The T-matrix method can also be used for scatterers with impedance boundary conditions, and for penetrable scatterers. For penetrable scatterers there is an induced interior field inside D and the boundary condition (4) is replaced by a transmission boundary condition.

The T-matrix method is based on expansion of the incident field and scattered field, respectively, in regular and radiating wavefunctions

$$\mathrm{Rg}\,\psi_n(r, \theta) = J_{|n|}(kr)e^{in\theta}, \tag{5}$$

$$\psi_n(r, \theta) = H^{(1)}_{|n|}(kr)e^{in\theta}, \tag{6}$$

for $n \in \mathbb{N}$. Here, J_n denotes the first kind Bessel function of order n and $H^{(1)}_n$ denotes the first kind Hankel function of order n. In particular, the expansions are

$$\psi^{\mathrm{inc}} = \sum_n f_n \,\mathrm{Rg}\,\psi_n, \tag{7}$$

$$\psi^{\mathrm{s}} = \sum_n a_n \,\psi_n, \tag{8}$$

where f_n and a_n denote expansion coefficients. Here, the summation is implicitly over $n \in \mathbb{N}$; later we abuse the same notation for truncated expansions of the fields. For

common incident fields such as plane waves or fields induced by point sources, the expansion coefficients $f = \{f_n\}$ are known and given explicitly [Colton and Kress 2012, Equations (3.88)–(3.89)] (see also Ganesh et al. [2012]). The unknown expansion coefficients $a = \{a_n\}$ of the scattered field are to be computed. The focus of this work is the numerically stable computation of these coefficients using standard double precision arithmetic, without any restriction on the shape and aspect ratio of the scatterer.

A consequence of the linearity of the Helmholtz equation (1) is that

$$a = Tf, \tag{9}$$

where $T = \{T_{mn}\}$ is called the T-matrix or transition matrix of D. The numerical stability of the computation of the unknown scattered field coefficients depends on the quality of the T-matrix. An appropriate metric is required to quantify the quality of the T-matrix.

In the sound soft and sound hard cases, the T-matrix satisfies the symmetry relation [Ganesh and Hawkins 2009, Theorem 1]

$$T + T^* - 2TT^* = 0. \tag{10}$$

Here, $*$ denotes the conjugate transpose. When the truncated T-matrix is computed numerically, the discrepancy in this relation yields a useful measure of the error. In our numerical results, we use the normalized discrepancy (see also Ganesh and Hawkins [2016, Section 8])

$$\frac{\|T + T^* - 2T\,T^*\|}{\|T\|}, \tag{11}$$

where for a finite dimensional matrix A,

$$\|A\| = \max_{n,m} |A_{nm}|.$$

In practice, the series expansions (7) and (8) are truncated for $|n| \leq N$ and the resulting truncated T-matrix is of size $(2N + 1) \times (2N + 1)$.

The celebrated Mie series for scattering by a spherical scatterer is a special case of the T-matrix method where the T-matrix is diagonal and the $2N + 1$ coefficients a_n for $|n| \leq N$ are known analytically. The rule of thumb [Wiscombe 1980] for a sphere of diameter $2R$ is to choose

$$N = \begin{cases} x + 4x^{1/3} + 1, & \text{for } x \leq 8, \\ x + 4.05\,x^{1/3} + 2, & \text{for } x < 4200, \\ x + 4x^{1/3} + 2, & \text{otherwise,} \end{cases} \tag{12}$$

where $x = 2\pi R/\lambda$ is proportional to the acoustic size Rk/π of the scatterer.

Numerical evidence inspired a conjecture that the required truncation parameter N for the T-matrix is independent of the shape of the scatterer, and hence the folklore that the empirical choice (12) is also appropriate for computing the T-matrix of nonspherical scatterers. Proving this conjecture was an open problem for several decades but was proven in Ganesh et al. [2012, Theorems 3.6 and 3.7] for the authors' numerically stable T-matrix formulation.

3. ORIGINAL FORMULATIONS FOR COMPUTING ENTRIES OF THE T-MATRIX

In Waterman's original formulation [Waterman 1969] the T-matrix is written

$$T = -(\mathrm{Rg}\,Q)\,Q^{-1}. \tag{13}$$

Waterman gave two alternative expressions for setting up the matrices $Q = \{Q_{mn}\}$ and $\mathrm{Rg}\,Q = \{\mathrm{Rg}\,Q_{mn}\}$.

First Expression. In the sound soft case

$$Q_{mn} = \frac{i}{4} \int_{\partial D} \frac{\partial}{\partial \boldsymbol{n}} (\text{Rg } \psi_n) \, \overline{\psi_m} \, ds, \tag{14}$$

$$\text{Rg } Q_{mn} = \frac{i}{4} \int_{\partial D} \frac{\partial}{\partial \boldsymbol{n}} (\text{Rg } \psi_n) \, \overline{\text{Rg } \psi_m} \, ds, \tag{15}$$

where $\boldsymbol{n}$ denotes the unit outward normal to the surface ∂D. In the sound hard case

$$Q_{mn} = \frac{i}{4} \int_{\partial D} \frac{\partial \overline{\psi_m}}{\partial \boldsymbol{n}} \, \text{Rg } \psi_n \, ds, \tag{16}$$

$$\text{Rg } Q_{mn} = \frac{i}{4} \int_{\partial D} \frac{\partial}{\partial \boldsymbol{n}} \overline{(\text{Rg } \psi_m)} \, \text{Rg } \psi_n \, ds. \tag{17}$$

Second Expression.

$$Q_{mn} = \frac{\sigma}{2} + \frac{i}{8} \int_{\partial D} \frac{\partial}{\partial \boldsymbol{n}} \left(\psi_n \, \overline{\text{Rg } \psi_m} \right) \, ds, \tag{18}$$

$$\text{Rg } Q_{mn} = \frac{i}{8} \int_{\partial D} \frac{\partial}{\partial \boldsymbol{n}} \left(\text{Rg } \psi_n \, \overline{\text{Rg } \psi_m} \right) \, ds, \tag{19}$$

where in the sound soft case $\sigma = 1$ and the sound hard case $\sigma = -1$.

Thus, in the sound soft case the T-matrix is computed using Equation (13) and either Equations (14) and (15) or Equations (18) and (19). In the sound hard case the T-matrix is computed using Equation (13) and either Equations (16) and (17) or Equations (18) and (19). Both of these methods for computing the T-matrix are called the NFM or extended boundary condition method.

Although for some geometries the boundary integrals in Equations (14)–(19) can be computed analytically, in general they must be computed numerically using appropriate quadrature over ∂D. The presence of the first kind Hankel function in the integrands of Equations (14), (16), and (18) can lead to loss of precision in evaluating the entries in Q using quadrature [Waterman 2007, 2009; Somerville et al. 2012; Havemann and Baran 2004]. This is because the Hankel function in the radiating wavefunction (6) grows unboundedly as n gets large and/or as r gets small. In practice, numerical difficulties also often arise with the inversion of the matrix Q in Equation (13), because the matrix is badly conditioned [Mishchenko and Travis 1994; Mishchenko et al. 1996; Petrov and Shkuratov 2007].

Numerical difficulties with the NFM have motivated alternative formulations for the T-matrix [Farafonov et al. 2010; Hellmers et al. 2011; Rother and Wauer 2010]. Substituting Equations (7) and (8) into the boundary condition (4) and requiring the boundary condition to hold at collocation points $\boldsymbol{z}_1, \ldots, \boldsymbol{z}_M \in \partial D$ yields

$$T = -H^{-1}J, \tag{20}$$

where $H = \{H_{jn}\}$, $J = \{J_{jn}\}$, and

$$H_{jn} = (\mathcal{D}\psi_n)(\boldsymbol{z}_j), \tag{21}$$

$$J_{jn} = (\mathcal{D} \, \text{Rg } \psi_n)(\boldsymbol{z}_j). \tag{22}$$

The number of collocation points M should be chosen according to the T-matrix truncation parameter N. If $M = 2N + 1$, then the matrices H and J are square and the

resulting method is known as the PMM. If $M > 2N+1$, then the inversion of H in Equation (20) should be replaced with a least squares solve, and the resulting method is known as the GPMM. The presence of the first kind Hankel function in Equation (21) leads to numerical difficulties similar to those arising in the NFM.

4. TMATROM FORMULATION FOR THE T-MATRIX

The expressions for the T-matrix in the NFM, PMM, and GPMM involve the Hankel function in the radiating wavefunction (6) evaluated on the boundary ∂D. The unbounded behavior of the Hankel function in the near field (on ∂D) is the cause of the numerical difficulties with these methods. The TMATROM package uses an alternative formulation developed by Ganesh and Hawkins [2010], Ganesh and Hawkins [2008a], and Ganesh and Hawkins [2009], in which the calculation of the T-matrix is moved from the near field to the far field (on the unit circle ∂B). The Hankel functions are bounded in the far field and hence the alternative formulation is numerically stable.

The TMATROM formulation involves using the regular wavefunctions $\mathrm{Rg}\,\psi_n$ individually as incident waves in the scattering problems (1)–(4). In particular, the interaction of the incident field $\psi^{\mathrm{inc}} = \mathrm{Rg}\,\psi_n$ with the scatterer through the boundary condition (4) induces a scattered field ψ^{s} satisfying Equations (1) and (2). Our T-matrix algorithm requires computation of the corresponding far field given by Equation (3), which we denote by ψ_n^∞ with the suffix indicating the association with the regular wavefunction $\mathrm{Rg}\,\psi_n$. Then the TMATROM T-matrix entries are given by Ganesh and Hawkins [2009]:

$$T_{mn} = \frac{1}{4}\sqrt{\frac{k}{\pi}}\,i^{|m|}(1+i)\int_{\partial B}\psi_n^\infty\,\overline{e_m}\,ds, \tag{23}$$

where $e_m(\theta) = e^{im\theta}$. In practice, the boundary integrals over ∂B in Equation (23) are computed numerically using the rectangle rule (which exhibits high-order convergence for periodic domains).

The far fields ψ_n^∞ induced by each regular wavefunction $\mathrm{Rg}\,\psi_n$ are computed numerically and any appropriate numerical solver can be used for this. Typically the appropriate numerical solver depends on the shape and material properties of the scatterer D. There are no restrictions on the shape of the scatterer provided an appropriate numerical solver is available. It is convenient to assume that the L_2 error in the numerically computed values of ψ_n^∞ is bounded by ϵ. Then the following convergence estimate follows from Ganesh et al. [2012, Theorem 3.9].

THEOREM 4.1. *For scattering of a plane wave by a scatterer of radius R,*

$$\|\psi^\infty - \psi_N^\infty\|_{L^2(\partial B)}^2 \le CN^2\left(\frac{Rke}{2N}\right)^{2N} + C'\epsilon^2, \tag{24}$$

provided the shape-independent T-matrix matrix truncation parameter $N > Rk/2 + 1$, where ψ_N^∞ is the far field computed using the truncated T-matrix with entries (23). Here $e = \exp(1)$ and C, C' are constants that are independent of N but may depend on D, R, and k.

The proviso that $N > Rk/2 + 1$ in Theorem 4.1 suggests that the truncation parameter N must grow with the radius R of the scatterer and with the wavenumber k. A consequence of Theorem 4.1 is that high-order convergence of the T-matrix method is preserved provided the far field induced by each regular wavefunction $\mathrm{Rg}\,\psi_n$ is evaluated with high-order accuracy by the forward solver. Such high-order forward solvers are well known in the two-dimensional case for smooth scatterers (see Colton and Kress [2012] and Barnett and Betcke [2010]) and for Lipschitz scatterers (see Barnett

Fig. 1.   Visualisations of our sound soft and sound hard test scatterers. The aspect ratio is in parentheses.

and Betcke [2010]) and these are supported in TMATROM. High-order forward solvers for the three-dimensional case are also available (see Wienert [1990], Bruno and Kunyansky [2001], and Ganesh and Graham [2004] for acoustics and Ganesh and Hawkins [2008b] for electromagnetism).

5. NUMERICAL EXPERIMENTS

We demonstrate the numerical stability of our TMATROM package by computing the T-matrix of several kinds of scatterer found in the literature and visualized in Figure 1. In the figure, and in subsequent tables, we indicate the aspect ratio of the scatterer (the width divided by the height or its reciprocal, as appropriate) in parentheses. In our experiments, we choose the wavenumber so that the scatterers have diameters between one wavelength and 100 wavelengths. We include results for both the sound soft and sound hard cases. Except where stated otherwise, in our experiments the T-matrix truncation parameter is given by Equation (12) incremented by 5.

   All of our experiments are performed in Matlab using double precision floating point arithmetic. It is well known that the accuracy of the NFM can be improved using extended precision arithmetic [Havemann and Baran 2004; Khlebtsov 2010; Mishchenko et al. 1996; Mishchenko and Travis 1994]. Extended precision arithmetic cannot be achieved in Matlab without using extensions and we do not use extended precision in any of our experiments. We show below that slower extended precision based computation is not required to achieve accurate solutions using TMATROM.

   Our test scatterers have been chosen to demonstrate the effects of changing aspect ratio (ellipses and capped cylinders [Sarkissian et al. 1993]), nonconvex shape (kite Colton and Kress [2012, Section 3.5]), and nonsmooth shape (hexagon). The

hexagon is particularly interesting because of its importance in atmospheric optics. All of the test scatterers are provided in the TMATROM installation (see Ganesh and Hawkins [2016, Section 9]).

TMATROM allows the user to choose from various forward scattering solvers (or to provide their own). For the ellipses, capped cylinders, and kite we use the Nyström method [Colton and Kress 2012, Section 3.5] with $2N_s + 2$ quadrature points to solve the combined single- and double-layer integral equation [Colton and Kress 2012, Equation (3.27)] in the sound soft case, and a similar combined layer equation [Kirsch and Monk 1994, Equation (3.5)] in the sound hard case.

For the ellipses and the kite, the Nyström method converges exponentially with respect to the Nyström parameter N_s because of the smooth boundary parametrisation. For the capped cylinders, the Nyström method converges only quadratically with respect to the Nyström parameter N_s due to the discontinuity in the derivative of the surface normal at the interfaces between the cylinder body and the circular caps.

For the hexagon we use the MPSPACK package [Barnett and Betcke 2014], which implements the method of fundamental solutions augmented with corner bases in a nonpolynomial finite element method [Barnett and Betcke 2010]. This method exhibits high-order convergence with respect to the number of corner bases and MFS points. The TMATROM package installation includes an interface to MPSPACK.

We compare the quality of the T-matrix computed using TMATROM with the T-matrices computed using the NFM, PMM, and GPMM using the normalized symmetry error (11). Motivated by Equation (24), we also obtain a direct measure of the error in the T-matrix using the relative far field error

$$\frac{\|\psi^\infty - \psi_N^\infty\|_{L^2(\partial B)}}{\|\psi^\infty\|_{L^2(\partial B)}}, \tag{25}$$

where ψ^∞ is the far field induced by the incident plane wave $\psi^{\text{inc}}(x, y) = e^{iky}$ and ψ_N^∞ is the approximation to the far field computed using the truncated T-matrix. In practice, the $L_2(\partial B)$ norms in Equation (25) are evaluated using the rectangle rule with 1,000 points and the reference far field ψ^∞ is computed numerically. We restrict use of the relative far field error (25) to the ellipse and capped cylinder geometries, for which we are able to compute the reference far field ψ^∞ accurately using a different solver than the one used in TMATROM to compute the T-matrix. In particular, for the ellipse and capped cylinder we compute the reference far field (directly, i.e., without using the T-matrix) using the MPSPACK package [Barnett and Betcke 2014], and hence this solver is completely independent of the Nyström method that we use to compute the T-matrix in TMATROM.

Boundary integrals in the NFM are computed using either M equally spaced points (ellipses and kite) or a composite Gauss-Legendre rule with M points (capped cylinder and hexagon). The number of intervals in the composite rule is fixed and the intervals are chosen so that points where the boundary is not smooth correspond to interval endpoints. In all cases, the number of quadrature points M in the NFM is proportional to the T-matrix truncation parameter. The PMM and GPMM are implemented with M equally spaced points with $M = 2N + 1$ in the PMM and $M = 4N + 2$ in the GPMM where N is the T-matrix truncation parameter.

Formulations of the NFM with enhanced numerical stability have been developed for the elliptical and capped cylinder scatterers [Waterman 2007, 2009; Sarkissian et al. 1993; Somerville et al. 2013]. We do not use these formulations here because they do not demonstrate typical behavior of the NFM for wider classes of scatterers, for which they are not applicable.

Table I. **Normalized Symmetry Error** (11) in the T-matrix
Computed Using the **Null Field Method** for Sound Soft Ellipses

Size	ellipse(1.1)	ellipse(1.5)	ellipse(3.0)	ellipse(6.0)
1.0	1.88e-15	1.03e-15	5.59e-02	6.14e+01
2.0	1.41e-15	1.29e-14	8.07e-01	1.96e+03
4.0	2.35e-15	3.95e-14	3.77e+01	1.50e+04
8.0	2.18e-15	1.30e-11	1.86e+02	1.12e+03
16.0	6.33e-14	7.41e-08	7.29e+04	5.02e+02

Table II. **Normalized Symmetry Error** (11) in the T-matrix
Computed Using the **Point Matching Method** for Sound
Soft Ellipses

Size	ellipse(1.1)	ellipse(1.5)	ellipse(3.0)	ellipse(6.0)
1.0	5.88e-09	6.68e-01	3.28e+01	1.30e+02
2.0	8.01e-09	2.00e+01	1.89e+03	9.41e+03
4.0	1.74e-08	5.48e+01	7.09e+06	3.47e+07
8.0	2.86e-07	1.48e+04	3.23e+11	5.59e+12
16.0	3.75e-05	5.23e+08	1.05e+15	6.78e+16

Table III. **Normalized Symmetry Error** (11) in the T-matrix
Computed Using the **Generalized Point Matching Method**
for Sound Soft Ellipses

Size	ellipse(1.1)	ellipse(1.5)	ellipse(3.0)	ellipse(6.0)
1.0	4.33e-11	4.31e-05	1.00e+00	1.00e+00
2.0	6.59e-11	1.20e-04	1.00e+00	1.00e+00
4.0	7.50e-11	5.14e-04	1.00e+00	1.00e+00
8.0	4.94e-10	2.85e-03	1.00e+00	1.00e+00
16.0	4.99e-09	4.10e-01	1.00e+00	1.00e+00

Effect of Aspect Ratio and Acoustic Size. We begin with numerical results for sound soft ellipses with aspect ratios between 1.1 and 6.0 to demonstrate the numerical instability that occurs in the NFM, PMM, and GPMM methods as the aspect ratio increases. Tables I–III show that in all three cases the normalized symmetry error (11) increases with aspect ratio and acoustic size. For large aspect ratios the normalized error in the GPMM is close to 1 because the computed T-matrix is close to zero. The numerical instability in the NFM is recognized in the literature to be due to cancellation error in the quadrature to compute the entries of Q and the large condition number of Q. The estimated error in Q is given in Table VII and the condition number of Q is given in Table VI. The corresponding error in Rg Q is less than 1e-14 in all cases. Similar ill conditioning is seen for the PMM and GPMM.

The error in the entries of Q is estimated by computing

$$\|Q - Q^{4M}\|, \tag{26}$$

where Q^{4M} denotes the matrix computed using four times as many quadrature points. The large errors observed in Table VII are associated with unbounded growth of the Hankel function $H_n^{(1)}(kr)$ in the radiating wavefunction (6) as n gets large and/or as r gets small. For example, for the scatterer ellipse(6.0) with acoustic size 16 wavelengths we have $kr = 16\pi/6$ at the minor radius of the ellipse and $|H_N^{(1)}(kr)| = 5.6\text{e}+56$ for truncation parameter $N = 72$.

In contrast to the results for the NFM, PMM, and GPMM in Tables I–III, Table IV shows that the normalized symmetry error for TMATROM remains small for all aspect ratios and acoustic sizes tested. In particular, for elongated ellipses (aspect ratios 3.0 and 6.0) the only method that can achieve symmetry error smaller than 1% is

Table IV. **Normalized Symmetry Error** (11) in the T-matrix
Computed Using **TMATROM** for Sound Soft Ellipses

Size	ellipse(1.1)	ellipse(1.5)	ellipse(3.0)	ellipse(6.0)
1.0	3.07e-14	6.50e-14	2.64e-09	3.54e-09
2.0	1.28e-10	6.04e-11	2.98e-11	4.82e-09
4.0	1.93e-11	8.86e-12	4.99e-11	7.73e-10
8.0	4.05e-10	1.60e-10	7.00e-10	7.42e-10
16.0	2.96e-09	1.00e-09	6.18e-09	6.90e-09

Table V. **Relative Far-Field Error** (25) in the T-matrix
Computed Using **TMATROM** for Sound Soft Ellipses

Size	ellipse(1.1)	ellipse(1.5)	ellipse(3.0)	ellipse(6.0)
1.0	4.44e-14	1.53e-12	1.59e-09	1.82e-09
2.0	8.17e-11	1.29e-11	7.00e-11	2.10e-09
4.0	2.38e-12	2.18e-11	1.84e-10	3.41e-10
8.0	5.94e-12	1.97e-10	1.39e-09	1.72e-09
16.0	1.72e-11	1.46e-09	8.48e-09	1.03e-08

Table VI. **Condition Number** of Q in the **Null Field Method**
for Sound Soft Ellipses

Size	ellipse(1.1)	ellipse(1.5)	ellipse(3.0)	ellipse(6.0)
1.0	3.82e+01	7.99e+00	5.89e+17	9.25e+30
2.0	4.58e+00	6.83e+01	3.06e+18	1.10e+37
4.0	8.60e+00	2.62e+01	4.13e+20	1.75e+48
8.0	9.42e+00	7.73e+01	1.02e+23	3.29e+59
16.0	3.72e+02	5.38e+03	5.02e+39	7.99e+81

TMATROM. The high accuracy attained by TMATROM is preserved for all acoustic sizes tested, even for the highest aspect ratio ellipse. Table V shows that the relative far-field error for TMATROM is consistent with the normalized symmetry error. Similar numerical experiments for sound hard ellipses yield qualitatively identical results to those in Tables I–VII.

Next, we give results for sound soft capped cylinders with the same aspect ratios used for the ellipse results above. The results in Tables VIII–X demonstrate similar numerical instability in the NFM, PMM, and GPMM as we observed for the ellipses. In contrast, Table XI shows that the normalized error using TMATROM remains small for all aspect ratios and acoustic sizes tested. (We refer to the comment below to explain the order of the error in the capped cylinder experiments.) TMATROM is the only method that does not fail for elongated capped cylinders (aspect ratios 3.0 and 6.0). In the case of the capped cylinder with aspect ratio 1.5, the NFM, PMM, and GPMM are stable only at small acoustic sizes. In contrast, stability of TMATROM is not conditional on acoustic size in the cases tested. Table XII shows that the relative far-field error for TMATROM is consistent with the normalised symmetry error. Similar numerical experiments for sound hard capped cylinders yield qualitatively identical results to those in Tables VIII–XII.

Detailed Results. Next, we give detailed results comparing the NFM, PMM, GPMM, and TMATROM methods for selected scatterers with high aspect ratio (ellipse and capped cylinder), nonconvex shape (kite), or nonsmooth shape (hexagon). Tables XIII–XVI show the normalized symmetry error for these sound soft scatterers with acoustic sizes between 1 and 16 wavelengths. The GPMM method gives a few percent accuracy for the kite, while the NFM, PMM, and GPMM all give about 0.1% accuracy for the hexagon. However, this accuracy is only attained for small acoustic size and the accuracy is much less at larger acoustic sizes. TMATROM exhibits significantly

Table VII. Estimated **Quadrature Error** in Q in the **Null Field Method** for Sound Soft Ellipses

Size	ellipse(1.1)	ellipse(1.5)	ellipse(3.0)	ellipse(6.0)
1.0	9.95e-08	1.38e-05	2.37e+08	3.90e+17
2.0	2.58e-08	1.34e-05	6.81e+08	5.90e+20
4.0	1.46e-07	3.50e-04	8.64e+09	5.99e+26
8.0	7.62e-08	9.36e-03	4.00e+11	5.88e+36
16.0	1.80e-07	1.26e+01	2.68e+21	1.07e+55

Table VIII. **Normalized Symmetry Error** (11) in the T-matrix Computed Using **NFM** for Sound Soft Capped Cylinders

Size	cylinder(1.1)	cylinder(1.5)	cylinder(3.0)	cylinder(6.0)
1.0	2.06e-04	3.40e-05	8.18e+00	2.20e+02
2.0	1.05e-05	8.98e-05	3.67e+02	1.97e+03
4.0	7.16e-06	1.35e-03	4.53e+03	9.54e+03
8.0	8.07e-05	1.19e-01	4.69e+05	2.12e+04
16.0	5.87e-06	8.33e+01	8.66e+07	1.61e+05

Table IX. **Normalized Symmetry Error** (11) in the T-matrix Computed Using **PMM** for Sound Soft Capped Cylinders

Size	cylinder(1.1)	cylinder(1.5)	cylinder(3.0)	cylinder(6.0)
1.0	5.77e-07	6.79e-04	2.74e+01	7.19e+01
2.0	4.82e-07	8.18e-03	8.13e+02	3.12e+03
4.0	5.17e-07	2.64e+00	2.18e+05	2.31e+06
8.0	7.19e-07	1.13e+03	4.57e+09	3.93e+11
16.0	2.02e-06	3.90e+05	3.39e+15	2.92e+16

Table X. **Normalized Symmetry Error** (11) in the T-matrix Computed Using **GPMM** for Sound Soft Capped Cylinders

Size	cylinder(1.1)	cylinder(1.5)	cylinder(3.0)	cylinder(6.0)
1.0	4.39e-07	6.28e-07	1.00e+00	1.00e+00
2.0	2.56e-07	9.57e-07	1.00e+00	1.00e+00
4.0	2.72e-07	4.60e-06	1.00e+00	1.00e+00
8.0	3.77e-07	6.70e-05	1.00e+00	1.00e+00
16.0	3.65e-07	1.00e+00	1.00e+00	1.00e+00

Table XI. **Normalized Symmetry Error** (11) in the T-matrix Computed Using **TMATROM** for Sound Soft Capped Cylinders

Size	cylinder(1.1)	cylinder(1.5)	cylinder(3.0)	cylinder(6.0)
1.0	3.04e-05	2.62e-05	2.26e-05	2.41e-05
2.0	1.69e-05	2.26e-05	2.46e-05	2.26e-05
4.0	1.97e-05	2.56e-05	2.37e-05	2.43e-05
8.0	2.21e-05	1.99e-05	2.44e-05	2.46e-05
16.0	1.73e-05	2.15e-05	2.43e-05	2.42e-05

Table XII. **Relative Far-Field Error** (25) in the T-matrix Computed Using **TMATROM** for Sound Soft Capped Cylinders

Size	cylinder(1.1)	cylinder(1.5)	cylinder(3.0)	cylinder(6.0)
1.0	2.54e-05	1.12e-05	6.25e-06	1.79e-05
2.0	1.22e-05	7.60e-06	1.08e-05	6.78e-06
4.0	2.02e-05	8.16e-06	7.22e-06	1.17e-05
8.0	2.13e-05	1.20e-05	5.18e-06	4.79e-06
16.0	1.75e-05	1.69e-05	8.18e-06	5.89e-06

Table XIII. Comparison of **Normalized Symmetry Error** (11) for All Methods for Sound Soft **ellipse(6.0)**

Size	TMATROM	NFM (M points)	NFM ($2M$ points)	NFM ($4M$ points)	PMM	GPMM
1.0	3.54e-09	6.14e+01	1.62e+01	1.93e-06	1.30e+02	1.00e+00
2.0	4.82e-10	1.96e+03	4.50e+01	1.32e-02	9.41e+03	1.00e+00
4.0	7.73e-10	1.50e+04	8.67e+03	8.27e+02	3.47e+07	1.00e+00
8.0	7.42e-10	1.12e+03	3.64e+05	2.00e+04	5.59e+12	1.00e+00
16.0	6.90e-09	5.02e+02	6.23e+03	2.45e+03	6.78e+16	1.00e+00

Table XIV. Comparison of **Normalized Symmetry Error** (11) for All Methods for Sound Soft **cylinder(6.0)**

Size	TMATROM	NFM (M points)	NFM ($2M$ points)	NFM ($4M$ points)	PMM	GPMM
1.0	2.41e-05	2.20e+02	1.79e+02	1.90e+01	7.19e+01	1.00e+00
2.0	2.26e-05	1.97e+03	3.91e+03	5.20e+02	3.12e+03	1.00e+00
4.0	2.43e-05	9.54e+03	6.13e+03	3.20e+03	2.31e+06	1.00e+00
8.0	2.46e-05	2.12e+04	3.52e+04	4.79e+03	3.93e+11	1.00e+00
16.0	2.42e-05	1.61e+05	6.29e+04	3.07e+05	2.92e+16	1.00e+00

Table XV. Comparison of **Normalized Symmetry Error** (11) for All Methods for Sound Soft **kite(1.2)**

Size	TMATROM	NFM (M points)	NFM ($2M$ points)	NFM ($4M$ points)	PMM	GPMM
1.0	3.89e-10	4.84e-01	4.84e-01	4.84e-01	8.63e+03	6.22e-02
2.0	2.87e-10	3.00e+01	3.00e+01	3.00e+01	4.12e+06	1.04e-01
4.0	6.26e-11	1.44e+01	1.44e+01	1.44e+01	9.88e+09	1.00e+00
8.0	2.39e-09	5.17e+01	5.17e+01	5.17e+01	7.04e+13	1.00e+00
16.0	5.49e-09	1.37e+03	1.09e+03	1.23e+03	5.30e+15	1.00e+00

Table XVI. Comparison of **Normalized Symmetry Error** (11) for All Methods for Sound Soft **hexagon(1.15)**

Size	TMATROM	NFM (M points)	NFM ($2M$ points)	NFM ($4M$ points)	PMM	GPMM
1.0	4.21e-09	2.94e-03	2.94e-03	2.94e-03	8.94e-04	3.12e-03
2.0	1.60e-09	8.74e-04	8.74e-04	8.74e-04	1.44e-03	5.86e-03
4.0	2.96e-09	9.56e+00	9.56e+00	9.56e+00	7.45e-03	9.62e-03
8.0	8.72e-09	1.04e+01	1.04e+01	1.04e+01	6.41e-02	2.00e-02
16.0	9.70e-09	8.03e+00	8.03e+00	8.03e+00	2.25e+01	3.74e-02

Table XVII. Comparison of **Relative Far-Field Error** (25) for All Methods for Sound Soft **ellipse(6.0)**

Size	TMATROM	NFM (M points)	NFM ($2M$ points)	NFM ($4M$ points)	PMM	GPMM
1.0	1.82e-09	1.93e+01	5.09e+00	3.41e-06	3.56e+01	1.00e+00
2.0	2.10e-09	4.96e+02	6.70e+00	2.33e-02	9.57e+02	1.00e+00
4.0	3.41e-10	1.20e+03	1.24e+03	4.57e+01	1.14e+06	1.00e+00
8.0	1.72e-09	1.74e+02	4.78e+04	1.08e+03	2.09e+10	1.00e+00
16.0	1.03e-08	5.55e+01	8.46e+02	1.45e+02	1.58e+14	1.00e+00

Table XVIII. Comparison of **Relative Far-Field Error** (25) for All Methods for Sound Soft **cylinder(6.0)**

Size	TMATROM	NFM (M points)	NFM ($2M$ points)	NFM ($4M$ points)	PMM	GPMM
1.0	1.79e-05	4.42e+01	4.27e+01	3.61e+00	4.58e+01	1.00e+00
2.0	6.78e-06	7.00e+01	5.50e+01	3.05e+01	1.81e+03	1.00e+00
4.0	1.17e-05	4.21e+02	2.94e+02	3.55e+01	4.69e+05	1.00e+00
8.0	4.79e-06	8.65e+02	1.86e+03	5.39e+02	1.68e+11	1.00e+00
16.0	5.89e-06	1.26e+04	8.87e+03	1.98e+04	1.72e+16	1.00e+00

Table XIX. Comparison of **Normalized Symmetry Error** (11) for All Methods for Sound Hard **ellipse(6.0)**

Size	TMATROM	NFM (M points)	NFM ($2M$ points)	NFM ($4M$ points)	PMM	GPMM
1.0	3.62e-09	1.08e+01	2.43e+00	7.68e-05	2.26e+01	1.00e+00
2.0	4.99e-09	3.69e+02	5.25e+01	1.88e-01	3.12e+03	1.00e+00
4.0	2.03e-09	4.75e+03	4.49e+02	7.22e+02	1.27e+07	1.00e+00
8.0	7.27e-10	2.85e+03	2.05e+05	6.82e+03	7.17e+12	1.00e+00
16.0	6.40e-09	8.71e+02	7.06e+03	3.99e+03	6.51e+15	1.00e+00

Table XX. Comparison of **Normalized Symmetry Error** (11) for All Methods for Sound Hard **cylinder(6.0)**

Size	TMATROM	NFM (M points)	NFM ($2M$ points)	NFM ($4M$ points)	PMM	GPMM
1.0	2.78e-05	3.03e+01	1.20e+01	1.36e+01	2.51e+01	1.00e+00
2.0	2.90e-05	4.75e+03	2.38e+03	1.23e+02	9.98e+02	1.00e+00
4.0	6.38e-05	2.09e+04	8.05e+03	1.15e+04	2.32e+06	1.00e+00
8.0	9.87e-05	5.62e+04	4.29e+04	5.10e+03	1.79e+11	1.00e+00
16.0	8.03e-05	6.42e+04	2.37e+05	2.08e+05	4.76e+16	1.00e+00

Table XXI. Comparison of **Normalized Symmetry Error** (11) for All Methods for Sound Hard **kite(1.2)**

Size	TMATROM	NFM (M points)	NFM ($2M$ points)	NFM ($4M$ points)	PMM	GPMM
1.0	7.15e-11	1.52e-01	1.52e-01	1.52e-01	2.12e+03	2.02e-01
2.0	1.16e-10	1.05e+01	1.05e+01	1.05e+01	7.35e+05	1.00e+00
4.0	7.40e-11	1.11e+01	1.11e+01	1.11e+01	6.34e+09	1.00e+00
8.0	7.21e-09	1.14e+02	1.14e+02	1.14e+02	1.22e+14	1.00e+00
16.0	2.65e-08	1.31e+03	8.25e+02	6.37e+02	7.12e+15	1.00e+00

higher accuracy than the NFM, PMM, and GPMM methods in all cases, even for larger acoustic sizes.

We have observed that in some cases the results for the NFM can be improved by increasing the quadrature degree (see also the discussion above and Table VII). Thus, for the NFM we include results obtained with the number of quadrature points doubled and quadrupled. The results in Tables XIII–XVI show that even quadruple quadrature degree is not sufficient to obtain robust stability for large aspect ratio or large acoustic size.

Tables XVII and XVIII show that in the case of the ellipse and the capped cylinder the far-field error exhibits similar features to those discussed above in the normalized symmetry error. Similar numerical experiments for sound hard scatterers are given in Tables XIX–XXIV and yield qualitatively similar results.

The error obtained with TMATROM is governed by the accuracy of the forward scattering solver. In most of our TMATROM results we chose the parameters for the forward scattering solver so that the normalized error in the sound soft case was less than 1e-08. For the capped cylinder we allow error larger than 1e-08 because of the slow convergence of the Nyström method due to the discontinuity in the derivative of the surface normal of this scatterer. The slow convergence in this case allows us to demonstrate how the error in the forward solver carries into the normalized error in the T-matrix. Table XXV shows the quadratic convergence of the normalized error in the T-matrix with respect to the Nyström parameter N_s for the sound soft case.

Performance. Next, we demonstrate the efficiency of TMATROM by comparing CPU times between the different methods. All CPU times were obtained using Matlab on a laptop computer with a quad core 2.6GHz CPU. The efficiency of TMATROM is governed by the efficiency of the forward scattering solver. In Table XXVI, we show the CPU time for the sound soft ellipse with aspect ratio 6.0. For this smooth scatterer the Nyström solver used by TMATROM is very efficient and the CPU time for the TMATROM method is very low. For the ellipse with acoustic size 16 wavelengths the

Table XXII. Comparison of **Normalized Symmetry Error** (11) for All Methods for Sound Hard **hexagon(1.15)**

Size	TMATROM	NFM (M points)	NFM ($2M$ points)	NFM ($4M$ points)	PMM	GPMM
1.0	3.76e-09	5.08e-04	5.09e-04	5.09e-04	1.50e-01	1.92e-01
2.0	3.37e-09	1.37e-03	1.37e-03	1.37e-03	1.23e-01	1.66e-01
4.0	2.23e-09	2.32e-03	2.32e-03	2.32e-03	3.24e-01	2.28e-01
8.0	5.11e-09	4.29e-03	4.29e-03	4.29e-03	1.33e+01	2.75e-01
16.0	1.50e-08	2.08e-02	2.08e-02	2.08e-02	1.07e+01	2.76e-01

Table XXIII. Comparison of **Relative Far-Field Error** (25) for All Methods for Sound Hard **ellipse(6.0)**

Size	TMATROM	NFM (M points)	NFM ($2M$ points)	NFM ($4M$ points)	PMM	GPMM
1.0	4.05e-09	4.85e+00	1.09e+00	7.40e-05	1.59e+01	1.00e+00
2.0	4.03e-09	1.15e+02	1.26e+01	1.65e-01	8.40e+02	1.00e+00
4.0	2.02e-09	2.56e+02	9.15e+01	2.21e+02	8.46e+05	1.00e+00
8.0	1.83e-09	5.36e+01	2.60e+04	5.60e+02	6.07e+10	1.00e+00
16.0	9.64e-09	3.49e+01	3.22e+02	2.48e+02	4.15e+13	1.00e+00

Table XXIV. Comparison of **Relative Far-Field Error** (25) for All Methods for Sound Hard **cylinder(6.0)**

Size	TMATROM	NFM (M points)	NFM ($2M$ points)	NFM ($4M$ points)	PMM	GPMM
1.0	1.17e-04	1.10e+01	8.56e+00	7.82e+00	4.29e+01	1.00e+00
2.0	9.04e-05	4.49e+01	3.93e+01	1.40e+01	5.81e+02	1.00e+00
4.0	1.03e-04	4.42e+02	4.97e+02	2.34e+02	5.72e+05	1.00e+00
8.0	1.14e-04	3.69e+03	4.83e+03	4.61e+02	5.69e+10	1.00e+00
16.0	9.50e-05	1.57e+04	2.08e+04	1.68e+04	9.09e+15	1.00e+00

Table XXV. **Normalized Symmetry Error** (11) in the T-matrix
Computed Using **TMATROM** with the Nyström
Solver with $2N_s + 2$ Points for Sound Soft **cylinder(6.0)**

		Normalized symmetry error		
Size	N_0	$N_s = \text{ceil}(N_0/2)$	$N_s = N_0$	$N_s = 2N_0$
1.0	145	3.94e-04	9.43e-05	2.41e-05
2.0	175	3.57e-04	9.04e-05	2.26e-05
4.0	205	3.93e-04	9.86e-05	2.43e-05
8.0	210	4.07e-04	9.94e-05	2.46e-05
16.0	290	3.88e-04	9.72e-05	2.42e-05

Table XXVI. Comparison of CPU Time (in Seconds) for All Methods for Sound Soft **ellipse(6.0)**

Size	TMATROM	NFM (M points)	NFM ($2M$ points)	NFM ($4M$ points)	PMM	GPMM
1.0	0.03	0.87	0.81	0.97	0.03	0.04
2.0	0.04	1.65	1.53	1.91	0.03	0.03
4.0	0.05	3.08	3.83	5.21	0.05	0.06
8.0	0.11	8.08	10.80	16.36	0.08	0.10
16.0	0.25	27.33	40.43	66.15	0.16	0.15

Table XXVII. Comparison of CPU Time (in Seconds) for All Methods for Sound Hard **hexagon(1.15)**.

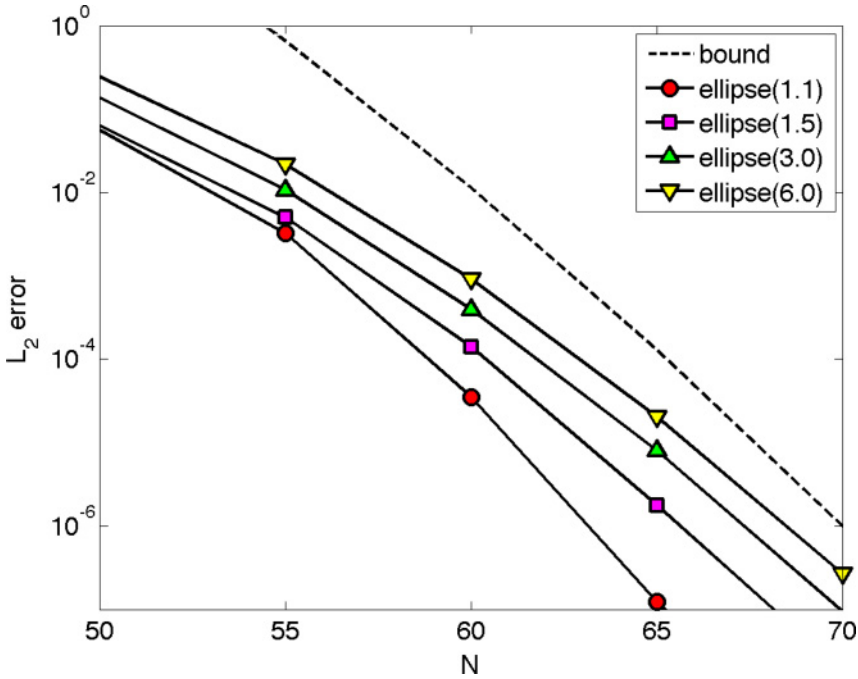| Size	TMATROM	NFM (M points)	NFM ($2M$ points)	NFM ($4M$ points)	PMM	GPMM
1.0	1.10	1.73	1.37	1.85	0.03	0.04
2.0	1.57	3.24	2.49	3.48	0.04	0.05
4.0	2.32	5.35	7.45	11.88	0.07	0.11
8.0	3.83	14.67	22.11	38.11	0.14	0.22
16.0	20.61	53.54	89.50	158.41	0.32	0.25

Fig. 2. $L_2(\partial B)$ error in the far field plotted against T-matrix truncation parameter N for ellipses with acoustic size 16 wavelengths. The far field is computed using the T-matrix for the incident plane wave $\psi^{\mathrm{inc}}(x, y) = e^{iky}$. The T-matrix is computed using TMATROM. The dashed line shows the theoretical convergence rate predicted by Equation (24).

CPU time to set up the Nyström matrix was 0.09 seconds. In Table XXVII we show the CPU time for the sound hard hexagon. For this polygonal scatterer the MPSPACK solver used by TMATROM involves several artificial domains and the CPU time is higher. However, in both cases the CPU time for TMATROM is much lower than the CPU time for the NFM. (TMATROM is shown to be the most accurate method for these experiments in Tables XIII and Table XXII).

In Figure 2, we demonstrate that the convergence rate of the far field computed using the truncated T-matrix is in agreement with the bound (24) by plotting the $L_2(\partial B)$ error of the far field against the truncation parameter N for ellipses having acoustic size 16 wavelengths. The truncated T-matrix used to compute the far field is computed using TMATROM. The reference far field is computed using MPSPACK as described above, and hence is completely independent from the T-matrix calculation. The far field is induced by the incident plane wave $\psi^{\mathrm{inc}}(x, y) = e^{iky}$. Similar figures are obtained for other acoustic sizes.

Finally, we demonstrate the stability of TMATROM for large acoustic sizes. In Table XXVIII we tabulate the normalized symmetry error (11) for T-matrices computed using TMATROM for sound soft ellipses with aspect ratios between 1.1 and 6.0 for acoustic sizes between 20 and 100 wavelengths. We highlight that TMATROM achieved normalized symmetry error smaller than 1e-08 in all cases, even for the ellipse with aspect ratio 6.0 and acoustic size 100 wavelengths (with $kR = 314.2$). None of the other methods tested could match this accuracy for this geometry even with acoustic size 1 wavelength.

Table XXVIII. **Normalized Symmetry Error** (11) in the T-matrix
Computed Using **TMATROM** for Sound Soft Ellipses

Size	ellipse(1.1)	ellipse(1.5)	ellipse(3.0)	ellipse(6.0)
20	4.41e-09	1.44e-09	3.93e-10	1.59e-10
40	3.02e-10	3.63e-09	8.85E-10	1.02e-09
60	8.44e-10	4.94e-09	2.50e-09	2.81e-09
80	1.39e-09	5.82e-09	5.71e-09	6.32e-09
100	2.05e-09	6.29e-09	8.48e-09	9.62e-09

ACKNOWLEDGMENTS

REFERENCES

A. H. Barnett and T. Betcke. 2014. MPSPACK Google Code Archive. Retrieved from https://code.google.com/p/mpspack/.

A. H. Barnett and T. Betcke. 2010. An exponentially convergent nonpolynomial finite element method for time-harmonic scattering from polygons. *SIAM J. Sci. Comp.* 32 (2010), 1417–1441.

L. Bi, P. Yang, G. W. Kattawar, and M. I. Mishchenko. 2013. Efficient implementation of the invariant imbedding T-matrix method and the separation of variables method applied to large nonspherical imhomogeneous particles. *J. Quant. Spectrosc. Radiat. Transfer* 116 (2013), 169–183.

O. P. Bruno and L. A. Kunyansky. 2001. A fast, high-order algorithm for the solution of surface scattering problems: Basic implementation, tests, and applications. *J. Comput. Phys.* 169 (2001), 80–110.

D. Colton and R. Kress. 2012. *Inverse Acoustic and Electromagnetic Scattering Theory*. Springer.

V. G. Farafonov, V. B. Il'in, and A. A. Vinokurov. 2010. Near- and far-field light scattering by nonspherical particles: Applicability of methods that involve a spherical basis. *Opt. Spectrosc.* 3 (2010), 432–443.

M. Ganesh and I. G. Graham. 2004. A high-order algorithm for obstacle scattering in three dimensions. *J. Comput. Phys.* 198 (2004), 211–242.

M. Ganesh and S. C. Hawkins. 2008a. A far-field based T-matrix method for three dimensional acoustic scattering. *ANZIAM J.* 50 (2008), C121–C136.

M. Ganesh and S. C. Hawkins. 2008b. A high-order tangential basis algorithm for electromagnetic scattering by curved surfaces. *J. Comput. Phys.* 227 (2008), 4543–4562.

M. Ganesh and S. C. Hawkins. 2009. A far-field based T-matrix method for two dimensional obstacle scattering. *ANZIAM J.* 51 (2009), C201–C216.

M. Ganesh and S. C. Hawkins. 2010. Three dimensional electromagnetic scattering T-matrix computations. *J. Comput. Appl. Math.* 234 (2010), 1702–1709.

M. Ganesh and S. C. Hawkins. 2013. A stochastic pseudospectral and T-matrix algorithm for acoustic scattering by a class of multiple particle configurations. *J. Quant. Spectrosc. Radiat. Transfer* 123 (2013), 41–52.

M. Ganesh and S. C. Hawkins. 2016. TMATROM: Object-Oriented T-matrix Reduced Order Model Software for Efficient Simulation of Multi-parameter Acoustic Scattering. Retrieved from http://www.mines.edu/mganesh/tmatrom_manual_curr.pdf.

M. Ganesh, S. C. Hawkins, and R. Hiptmair. 2012. Convergence analysis with parameter estimates for a reduced basis acoustic scattering T-matrix method. *IMA J. Numer. Anal.* 32 (2012), 1348–1374.

S. Havemann and A. J. Baran. 2004. Calculation of the phase matrix elements of elongated hexagonal ice columns using the T-matrix method. *J. Quant. Spectrosc. Radiat. Transfer* 89 (2004), 87–96.

J. Hellmers, V. Schmidt, and T. Wriedt. 2011. Improving the numerical stability of T-matrix light scattering calculations for extreme particle shapes using the nullfield method with discrete sources. *J. Quant. Spectrosc. Radiat. Transfer* 112 (2011), 1679–1686.

H. Kagemoto and D. K. P. Yue. 1986. Interactions among multiple three-dimensional bodies in water waves: An exact algebraic method. *J. Fluid Mech.* 166 (1986), 189–209.

N. Khlebtsov. 2010. Anisotropic properties of plasmonic nanoparticles: Depolarized light scattering, dichroism, and birefringence. *J. Nanophotonics* 4 (2010), 041587.

A. Kirsch and P. Monk. 1994. An analysis of the coupling of finite-element and Nyström methods in acoustic scattering. *IMA J. Numer. Anal.* 14 (1994), 523–544.

D. J. Little, S. C. Hawkins, and D. M. Kane. 2015. An exact surface-integral approach for accurate interferometric microscopy of single nanoparticles. *Opt. Express* 23 (2015), 6228–6238.

M. I. Mishchenko. 2016. T-matrix codes for computing electromagnetic scattering by non spherical and aggregated particles. Retrieved from http://www.giss.nasa.gov/staff/mmishchenko/t_matrix.html.

P. A. Martin. 2003. On connections between boundary integral equations and T-matrix methods. *Eng. Anal. Bound. Elem.* 27 (2003), 771–777.

R. C. McPhedran, L. C. Botten, A. A. Asatryan, N. A. Nicorovici, P. A. Robinson, and C. M. de Sterke. 1999. Calculation of electromagnetic properties of regular and random arrays of metallic and dielectric cylinders. *Phys. Rev. E* 60 (1999), 7614–7617.

M. I. Mishchenko. 2000. Calculation of the amplitude matrix for a nonspherical particle in a fixed orientation. *Appl. Opt.* 39 (2000), 1026–1031.

M. I. Mishchenko and others. 2014. Comprehensive thematic T-matrix reference database: A 2013–2014 update. *J. Quant. Spectrosc. Radiat. Transfer* 146 (2014), 249–354.

M. I. Mishchenko and L. D. Travis. 1994. T-matrix computations of light scattering by large spheroidal particles. *Opt. Commun.* 109 (1994), 16–21.

M. I. Mishchenko and L. D. Travis. 2007. Capabilities and limitations of a current Fortan implementation of the T-matrix method for randomly oriented, rotationally symmetric scatterers. *J. Quant. Spectrosc. Radiat. Transfer* 60 (2007), 309–324.

M. I. Mishchenko, L. D. Travis, and D. W. Mackowski. 1996. T-matrix computations of light scattering by nonspherical particles: A review. *J. Quant. Spectrosc. Radiat. Transfer* 55 (1996), 535–575.

F. Montiel, V. A. Squire, and L. G. Bennetts. 2015. Evolution of directional wave spectra through finite regular and randomly perturbed arrays of scatterers. *SIAM J. Appl. Math.* 75 (2015), 630–651.

T. A. Nieminen. 2014. Software projects. Retrieved from http://www.physics.uq.edu.au/people/nieminen/software.html.

T. A. Nieminen, V. L. Y. Loke, A. B. Stilgoe, G. Knöner, A. M. Brańczyk, N. R. Heckenberg, and H. Rubinsztein-Dunlop. 2007. Optical tweezers computational toolbox. *J. Opt. A* 9 (2007), S196–S203.

T. A. Nieminen, H. Rubinsztein-Dunlop, and N. R. Heckenberg. 2003. Calculation of the T-matrix: General considerations and application of the point-matching method. *J. Quant. Spectrosc. Radiat. Transfer* 79 (2003), 1019–1029.

D. Petrov and Y. Shkuratov. 2007. Optimized matrix inversion technique for the T-matrix method. *Opt. Lett.* 32 (2007), 1168–1170.

W. M. Robertson and J. F. Rudy III. 1998. Measurement of acoustic stop bands in two-dimensional periodic scattering arrays. *J. Acoust. Soc. Am.* 104 (1998), 694–699.

T. Rother and J. Wauer. 2010. Case study about the accuracy behaviour of three different T-matrix methods. *Appl. Opt.* 49 (2010), 5746–5756.

A. Sarkissian, C. F. Gaumond, and L. R. Dragonette. 1993. T-matrix implementation of forward scattering from rigid structures. *J. Acoust. Soc. Am.* 94 (1993), 3448–3453.

Scattport. 2016. Homepage. Retrieved from http://www.scattport.org.

W. R. C. Somerville, B. Auguié, and E. C. Le Ru. 2012. Severe loss of precision in calculations of T-matrix integrals. *J. Quant. Spectrosc. Radiat. Transfer* 113 (2012), 524–535.

W. R. C. Somerville, B. Auguié, and E. C. Le Ru. 2013. A new numerically stable implementation of the T-matrix method for electromagnetic scattering by spheroidal particles. *J. Quant. Spectrosc. Radiat. Transfer* 123 (2013), 153–168.

W. R. C. Somerville, B. Auguié, and E. C. Le Ru. 2016. SMARTIES. Retrieved from http://www.victoria.ac.nz/scps/research/research-groups/raman-lab/numerical-tools/smarties.

L. Tao, H. Song, and S. Chakrabarti. 2007. Scaled boundary FEM solution of short-crested wave diffraction by a vertical cylinder. *Comput. Meth. Appl. Mech. Eng.* 197 (2007), 232–242.

P. C. Waterman. 1965. Matrix formulation of electromagnetic scattering. *Proc. IEEE* 53 (1965), 805–812.

P. C. Waterman. 1969. New formulation of acoustic scattering. *J. Acoust. Soc. Am.* 45 (1969), 1417–1429.

P. C. Waterman. 1999. Surface fields and the T matrix. *J. Opt. Soc. Am. A* 16 (1999), 2968–2977.

P. C. Waterman. 2007. The T-matrix revisited. *J. Opt. Soc. Am. A* 24 (2007), 2257–2267.

P. C. Waterman. 2009. T-matrix methods in acoustic scattering. *J. Acoust. Soc. Am.* 125 (2009), 42–51.

L. Wienert. 1990. *Die Numerische Approximation von Randintegraloperatoren für die Helmholtzgleichung im $\mathbb{R}^3$.* Ph.D. Dissertation. University of Göttingen.

W. J. Wiscombe. 1980. Improved Mie scattering algorithms. *Appl. Opt.* 19 (1980), 1505–1509.

T. Wriedt. 2007. Review of the null-field method with discrete sources. *J. Quant. Spectrosc. Radiat. Transfer* 106 (2007), 535–545.

T. Wriedt. 2010. Null-field Method with Discrete Sources (NFM-DS). Retrieved from http://www.scattport.org/index.php/programs-menu/t-matrix-codes-menu/239-nfm-ds.